JOURNAL OF PROPULSION AND POWER
Vol. 33, No. 3, May–June 2017

Recommended Practice for Pressure Measurement and Calculation of Effective Pumping Speed in Electric Propulsion Testing

John W. Dankanich*
NASA Marshall Space Flight Center, Huntsville, Alabama 35812
Mitchell Walker†
Georgia Institute of Technology, Atlanta, Georgia 30332
and
Michael W. Swiatek‡ and John T. Yim§
NASA Glenn Research Center, Cleveland, Ohio 44135

DOI: 10.2514/1.B35478

The electric propulsion community has been implored to establish and implement a set of universally applicable test standards during the research, development, and qualification of electric propulsion systems. Variability between facility-to-facility and more importantly ground-to-flight performance can result in large margins in application or aversion to mission infusion. Performance measurements and life testing under appropriate conditions can be costly and lengthy. Measurement practices must be consistent, accurate, and repeatable. Additionally, the measurements must be universally transportable across facilities throughout the development, qualification, spacecraft integration, and on-orbit performance. A recommended practice for making pressure measurements, pressure diagnostics, and calculating effective pumping speeds with justification is presented.

Nomenclature

A_e	=	cross-sectional area of the electron beam, cm^2
A_σ	=	collective ionization cross area, cm^2
a	=	Clausing transmission coefficient
C	=	conductance, l/s
$C_{\text{Subscript}}$	=	conductance of the element, l/s
C_M	=	molecular conductance
D	=	diameter, m
e	=	electron charge, eV
k	=	pumping speed reduction factor
κ	=	Boltzmann constant, 1.38064×10^{-23} J/K
L	=	length, m
I_C	=	collector current, A
I_e	=	electron current, A
I_R	=	molecular impact rate, impacts/cm^2
I_S	=	molecular Impacts with a surface, atoms/($cm^2 \cdot s$)
M	=	molar mass, g/mol
$\dot{m}$	=	flow rate, (torr · l)/s
N	=	number of electrons
N_v	=	number of moles in the volume
n	=	molecular density, kg/m^3
P	=	pressure, Pa
p	=	pressure, torr
R_g	=	gauge relative sensitivity factor
S	=	gauge sensitivity factor, $torr^{-1}$
T	=	temperature, K
V	=	volumetric flow rate, l/($cm^2 \cdot s$)
V_g	=	grid potential, V_{dc}
σ_i	=	ionization cross section, m^2

Presented as Paper 2012-3737 at the 48th AIAA/ASME/SAE/ASEE Joint Propulsion Conference Exhibit, Atlanta, GA, 30 July–01 August 2012; received 2 June 2014; revision received 29 February 2016; accepted for publication 14 March 2016; published online 2 August 2016.

*Project Manager, Technology Development and Transfer, ZP30. Associate Fellow AIAA.
†Associate Professor, High-Power Electric Propulsion Laboratory, 449 Guggenheim. Associate Fellow AIAA.
‡Vacuum Systems Engineer, Space Power and Propulsion, M/S 301-3.
§Aerospace Engineer, In-Space Propulsion Systems Branch, M/S 86. Member AIAA.

I. Introduction

THE acknowledgment of challenges associated with accurate, consistent, repeatable, and transportable test results of electric propulsion systems has been well documented in recent years [1]. As such, there has been significant interest in developing rigorous standards for electric propulsion testing from both internal and external communities. Several community efforts including the European Space Agency [2], the Joint Army Navy NASA Air Force Committee on Electric Propulsion Diagnostics, and AIAA have begun efforts to "standardize" practices and measurements during the testing of electric propulsion devices.

Variability between facility-to-facility and (more importantly) ground-to-flight performance can result in large margins in application or aversion to mission infusion. Performance measurements and life testing under appropriate conditions can be both costly and lengthy (greater than 7000 h) [3]. Measurement practices must be consistent, accurate, and repeatable. Additionally, the measurements must be universally transportable across facilities throughout the development, qualification, spacecraft integration, and on-orbit performance. Critical to transportable measurements is the understanding and influence of facility effects. Background pressure is one of the primary facility effects well documented to influence ground-test results [4].

This paper describes a recommended practice for measuring pressure and calculating neutral density and effective pumping speeds during electric propulsion testing. A universal theory for an a priori prediction of the influence of facility effects for all thrusters is incomplete. Consequently, these recommendations are intended to evolve as the community continues to develop new theories, modeling capabilities, and practices.

II. Pressure Gauge Description and Operation

This section summarizes a recommended gauge design and practices for the purpose of pressure measurements and neutral density calculations in vacuum systems over the range of interest of electric propulsion testing. This is acknowledged only to be a first iteration with the community, and applicability is intentionally limited to gridded-ion and Hall thrusters. The pressure measurements of the

recommended gauge are applicable over the general range of 10^{-8} to 10^{-4} torr for N_2 or air.

Vacuum pressure gauges measure pressure from 10^{-16} torr to atmospheric. No single measurement technique can accurately measure over this entire range. Instead, various types of gauges are available for the specific range of interest. Higher pressure ranges, greater than or equal to 10^{-4} torr, can be accommodated with techniques relying on mechanical deflection or thermal conductivities including thermocouple gauges, diaphragms, liquid manometers, etc. In the lower pressure range, measurement techniques often rely on the collection of ions generated from the ambient gas to measure the neutral density, which is then converted to pressure. High-vacuum gauges include cold cathode ionization gauges, hot-cathode (Bayard–Alpert) ionization gauges, and spinning rotor gauges. Description and comparison of the various gauges are available in open literature. For brevity, this paper is limited to the recommended gauge: the Bayard–Alpert (BA) hot-cathode ionization gauge. The hot-cathode BA gauge is recommended for electric propulsion testing over cold cathode gauges due to the higher inaccuracy of the latter and over spinning rotor gauges with better performance but practical limitations in an environment with sputtered materials [5]. The principles, design, use, and limitations of BA gauges have been previously documented [6].

A. Bayard–Alpert Hot-Cathode Gauge Theory

All BA gauges consist of a heated cathode filament, an acceleration grid, and a grounded collector, as shown in Fig. 1. The individual elements of a BA gauge are described and illustrated in Sec. II.B and Figs. 2–4 [7]. The thermionic cathode filament is heated and emits electrons. The electrons are accelerated by a grid into the ionization region. The electrons collide with and ionize ambient neutral particles that enter the gauge. Those ions are collected by a grounded ion collector, and the measured current is linearly proportional to the number density of the gas. The positive ion current provides an indirect measurement of the gas pressure.

1. *Basic Operating Principles*

The pressure measurement via the collection current is a function of the number of molecules per unit volume, the ionization cross section for the gas of interest at the appropriate electron energy, the emission current, and the path length of the electrons [8]. Using the ionization cross section σ_i, length of the ionizing space (L), and cross-sectional area of the electron beam (A_e), we can use the molecular density n to determine the number of molecules in the volume:

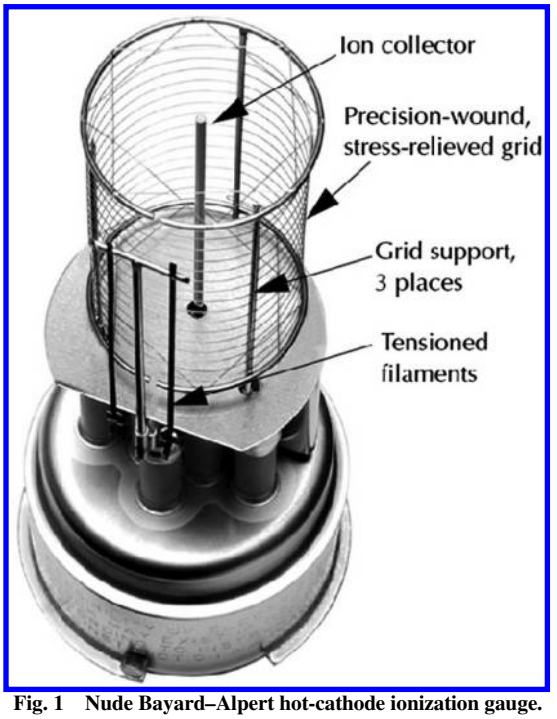

Fig. 1 Nude Bayard–Alpert hot-cathode ionization gauge.

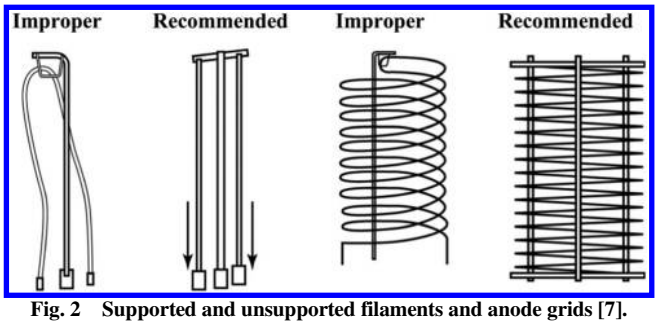

Fig. 2 Supported and unsupported filaments and anode grids [7].

$$N_V = n\,L\,A_e \tag{1}$$

Using the ideal gas law,

$$n = \frac{P}{kT} \tag{2}$$

The total ionization cross-sectional area of the molecules within the volume is

$$A_\sigma = nLA_e\sigma_i = \frac{LA_e\sigma_i P}{kT} \tag{3}$$

and the fraction of incoming electrons that participate in the ionizing collisions is

$$\frac{A_\sigma}{A_e} = n\,L\,\sigma_i = \frac{L\,\sigma_i\,P}{kT} \tag{4}$$

If N is the number of electrons entering the anode grid per unit time, then the number of collisions per unit time is

$$\frac{NL\sigma_i P}{kT} \tag{5}$$

Finally, assuming efficient collection and electron charge e, the collector current will be

$$I_c = NL\sigma_i\left[\frac{P}{kT}\right]e \tag{6}$$

Substituting for the electron emission current, $I_e = Ne$, we obtain the expression

$$I_c = \left[\frac{L\sigma_i}{kT}\right]\cdot I_e \cdot P \tag{7}$$

The first term of Eq. (7) is a function of the gas type, the geometry of the gauge, and the temperature, typically defined as the gauge sensitivity factor S, yielding the standard ionization gauge equation:

$$I_c = SI_eP \quad \text{or} \quad \text{Sensivity} = \frac{\text{Ion Current}}{\text{Electric Current}\cdot\text{Pressure}} \tag{8}$$

It is the linear relationship between pressure and the ion current that allows the Bayard–Alpert gauge to provide an accurate continuous indicator of pressure over the range of interest to electric propulsion testing. The BA gauge will deviate from linearity at higher pressure, but not below 10^{-4} torr [9]. The linear range can be extended to higher pressures by lowering the electron emission current. There are several methods and factors for using BA gauges at higher pressures, but they are beyond the scope of this paper. It should also be noted that this linearity at low pressures allows the BA gauge to be calibrated in the linear region and extends its performance range

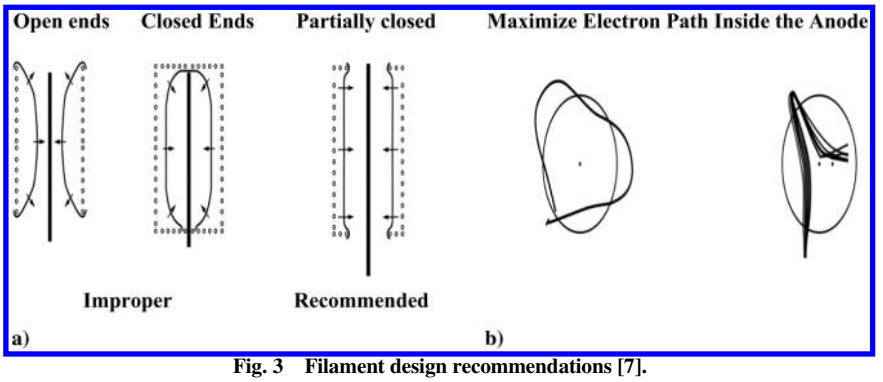

Fig. 3 Filament design recommendations [7].

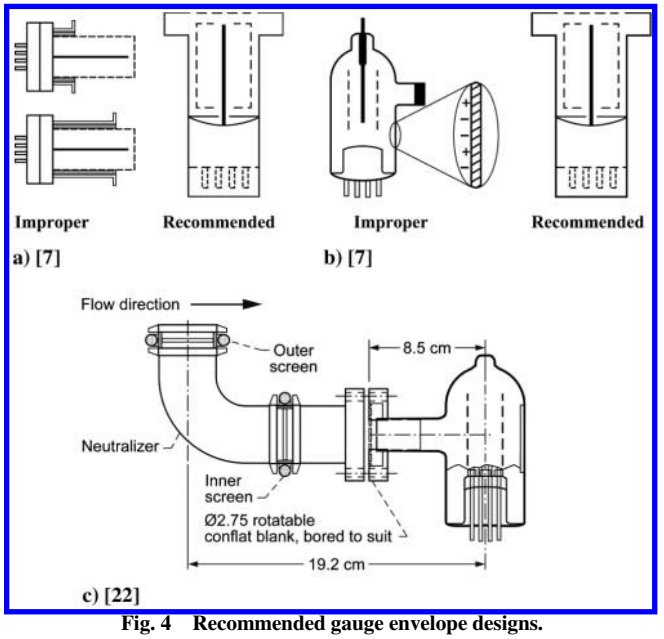

Fig. 4 Recommended gauge envelope designs.

below the calibration levels. This methodology has been confirmed down to 10^{-9} torr with pressure dependencies well characterized [10]. Dependency on gas, gauge voltages, temperature, and magnetic fields is briefly discussed in the following sections.

2. *Gas Dependency*

The BA gauge sensitivity, directly related to the value of the ionization cross section of the corresponding gas molecules and the sensitivity factor of the gauge, is only valid for the gas specified. The pressure readout only provides a direct reading for that gas. The industry standard gas is nitrogen. All gauges include relative sensitivity factors R_g and are commonly referred to as gas correction factors. The typical correction factors are noted in Sec. IV.C. Gas correction factors are pressure-dependent and can become unreliable above 10^{-5} torr [11]. Although this is not a significant concern for xenon in the range of electric propulsion testing, higher precision is obtained through calibration against the specific gas used during testing.

3. *Bias Voltage and Emission Current Dependence*

Collector current is a function of the electrode potentials because both the electron trajectories and ionization efficiencies depend on these voltages. Table 1 provides recommended gauge potentials [12]. The sensitivity of an ion gauge can change by 0.1 and 1%/V for filament-to-grid and filament-to-ground variations in potential, respectively.

Table 1 Recommended electrode potentials [12]

Parameter	Value
Collector potential	0 V_{dc}
Filament bias	+30 V_{dc}
Anode grid bias	+150 – 180 V_{dc}
Shield potential	0 V_{dc}

Although only 5 V_{dc} is required for the filament bias, the recommended positive filament bias of 30 V_{dc} is to assure that no electrons contact the ion collector. Increases in collector voltage are undesired and decrease the ion current due to reduced path length and electron penetration into the anode grid space and the reduced electron energy. Cathode bias should be applied to the bottom of the filament.

The filament-to-anode voltage determines the collisional energy of the electrons that traverse the inner volume of the grid cage. The electron energy is simply calculated, in electron volts, as the difference in bias voltage between the anode grid and the filament. The electron energy for the prototypical ion gauge controller is 150 eV. If the collector current is measured for varying grid potentials at a fixed pressure (above 10^{-7} torr), filament bias, and electron current, the curve showing I_c versus V_g follows the expected characteristic shape of gas ionization probability versus electron impact energy. The ionization current rises rapidly with V_g up to 200 V and varies slowly with grid voltages above this value [13].

Sensitivity is also dependent on the emission current. Emission currents ranging from 0.1 to 1 mA usually show no degradation. Increasing emission currents to 10 mA can decrease sensitivity by 20% and cause nonlinearity above 10^{-5} torr. BA gauges should be operated with 1 mA emission current. Higher current should only be used to increase the speed of outgassing. The filament current supply should be dc. The controller should control bias voltages within a few volts directly at the gauge head, and emission currents should be controlled to within a few percent [14,15]. If the bias voltage is controlled within the gauge controller, the voltage can vary with heating current due to resistive voltage drop across the cable and vary with cable length. The filament bias voltage should be controlled at the gauge head and not the controller box.

4. *Temperature Dependency*

The hot-cathode ionization gauge must obtain thermal equilibrium internally and with its surrounding before accurate pressure measurements can be made. This process can be accelerated with the use of the degassing feature on most commercial hot-cathode ionization gauge systems.

The hot-cathode ionization gauge should be operating for more than 1 h and should operate for 2 h before experimental measurements are taken to ensure thermal equilibrium is reached and outgassing of the surfaces is complete. The gauge should operate for at least 1 h after a degas event before making measurements [6]. For critical testing, it is recommended to operate the gauge several hours, typically overnight before making measurements.

Studies of temperature effect on results have shown that there is lower practical accuracy impact than theoretical analyses would predict when accounting for both density and thermal transpiration [16]. The envelope temperature of the BA gauge will typically be much higher than ambient due to the power radiated by the hot filament and absorbed by the walls of the envelope. The absorption of energy from the filament by the envelope increases with age as the

walls get progressively darker due to contamination. Variations in filament work function and emissivity due to aging, contamination, or chemical reaction with the gas will result in changes in filament and envelope temperature that might require correction for accurate measurements.

Studies have shown the ion current to change by 0.075%/K, approximately half of that expected from the envelope temperature [17]. Sensitivity changes can be mitigated though calibration under the same temperature as those during the test. If a large variation is expected, a correction may be required. A temperature-correction methodology is provided in Sec. IV.D.4.

5. *Magnetic Field Dependency*

Magnetic fields near BA gauges can significantly impact performance by affecting the trajectories of the charged particles. The effects are nonlinear with both magnetic field and pressure. However, no conclusive study has been completed to characterize the magnetic field effect on pressure measurement accuracy. If following gauge placement recommendations in Sec. IV, the performance change should be negligible. If a gauge is placed relatively close to a magnetic field source, testing the gauge with and without the expected magnetic field is recommended. The recommended practice would be to achieve a gyroradius at least an order of magnitude greater than the diameter of the gauge such that the particles would be effectively unmagnetized and local magnetic field dependency inside the gauge is mitigated [18].

B. Gauge Construction

The standard Bayard–Alpert hot-cathode gauge is the most prevalent pressure gauge used during electric propulsion testing. The hot-cathode BA gauge is generally considered the most accurate continuous indicator for pressure below 10^{-3} torr. Vendors specify typical accuracies of $\pm 20\%$, but 30–50% total uncertainty has been historically demonstrated, and the gauges exhibit limited stability required for test-to-test repeatability. A study on long-term stability (580 days) of BA gauges observed changes in calibration that ranged from −57 to 72% [19]. Follow-on studies highlighted the influence of the controller on uncertainty, and with a quality controller and proper calibration procedures, accuracies of $\pm 20\%$ can be achieved. However, design and construction techniques can significantly improve both the accuracy and stability of the pressure measurements [20]. Individually calibrated high-accuracy gauges offer accuracies better than 4% over the range most applicable to electric propulsion testing.

1. *Gauge Geometry Dependency*

The key geometry factors of gauge design include the filament-to-grid spacing, the collector wire location and diameter, the anode grid end closures, and the grid diameter. It is also the variations and change in these parameters over time that impact gauge-to-gauge variability and stability, respectively.

Standard BA gauges are known to exhibit large inaccuracies and instabilities due to gauge construction limitations. BA gauge filaments and grids can sag or change shape due to thermal cycling and even placement. The preferred mounting orientation is with the filament and anode grid in a vertical position to minimize the electrode distortion caused by gravity pull and thermal cycles. Gauges with opposed tungsten filaments have better long-term stability by a factor of 2. One should use all-metal gauges if there will be helium leak testing due to the heated glass permeation of helium. Gauges should be designed to support both the filament and the acceleration grid. Supported elements can eliminate the preference for vertical mounting and reduce gauge placement limitations, as shown in Fig. 2. Tight cathode filaments stretched between rigid posts have longer-term stability over hairpin-shaped or unsupported ribbon cathodes.

Another source of variations is the electrode position precision. Variations in placement can impact the electron collection, resulting in measurement inconsistencies. To maintain stability over the entire pressure range, it is also desired to have a thicker-diameter ion collector. The thicker wire provides increased mechanical stability and higher overall sensitivity. Increasing the collector-wire diameter from 0.25 to 1 mm will increase the sensitivity by a factor of 2. The ion collector should be approximately 1 mm in diameter. Ultrahigh vacuum gauges typically use smaller diameter collectors and should be avoided. The only disadvantage to the thicker (1 mm) wire is a higher sensitivity to the energetic ions formed by electron-stimulated desorption, avoidable through bakeout and degas.

Filaments should be sized and placed for emission of electrons in the radial electric field region to minimize the axial field effects on the electron paths, as shown in Fig. 3a. The filaments should also be designed to maximize the electron path to be within the anode grid, as shown in Fig. 3b. Last, the addition of grid-end closures, as in Fig. 3a, to the gauge will prevent the escape of uncaptured ions from the opened ends of the cylindrical grid and increase sensitivity, as in Fig. 3a. The sensitivity advantage declines rapidly above 10^{-5} torr, but open-end grids would only be recommended if testing occurred in pressure ranges up to 10^{-3} torr.

2. *Gauge Envelope Dependence (Nude Gauges)*

The envelope size and shape have been studied extensively for conventional nude BA gauges [21]. The results show that changes in the gauge envelope can result in measurement errors of 50%. Modern high-accuracy gauges rely on heavy shielding to protect the electrode from external and uncontrollable fields, better define charged particle trajectories, and improve both the gauge-to-gauge reproducibility and long-term stability.

It is critical to maintain a consistent electric environment during testing. Gauges can house the entire electrode assembly in a grounded metal envelope that completely surrounds the structure (Fig. 4a) to provide a stable electric environment for charged particle trajectories. A grounded, perforated, high-conductance shield over the port can electrically isolate the electrode structures from the rest of the vacuum system. A grounded conducting shield between the anode and the feedthrough prevents the ceramic insulators from becoming contaminated and charged (Fig. 4b).

Diagnostic locations and/or facility constraints may require pressure measurements within the plume of a thruster. The pressure levels will still be in the high vacuum range; thus, ionization gauges are necessary. However, because of the abundant presence of plume ions, the gauge will have high uncertainty if directly exposed to the plasma. If the gauge must be exposed to the plasma, a neutralizer should be installed on the gauge to prevent discharge ion collection by the gauge. The neutralizer should prevent line of sight to the hot plasma and be grounded to provide means for neutralization of discharge ions. Nude gauges can have higher accuracies by eliminating conductance losses; however, because shielded gauges can prevent the false measurement of collecting electrons from the plasma generated by the thruster, they may be required. The conductance losses of the neutralizer should be minimized and should be included in the pressure calculation and gauge calibration. The screen spacing should be sized smaller than five Debye lengths so that the sheath merges. An example setup is provided in Fig. 4c.

Commercial products are available that meet the aforementioned recommendations, such as the Granville-Phillips Stabil-ion Gauge model 370120 with either an IGC100 or Granville-Phillips Series 370 controller. This information is given as convenience and does not constitute an endorsement. Equivalent products may be used if they can be shown to produce consistence results, or the uncertainty analysis must reflect the inaccuracies and sources.

3. *Filament Design*

The filament design and material are critical to supply a stable electron emission current source and, therefore, high-accuracy measurements. The desired characteristics of the filaments are to have a reduced chemical reactivity with the rarefied environment to be measured, reduced evaporation rate at the operating temperature for prolonged life, a vapor pressure at least one order of magnitude lower than that measured, and low levels of outgassing.

Filament materials used in BA gauges are either pure metal (e.g., tungsten) or oxide-coated (e.g., thoria-coated iridium). The operating temperature of tungsten cathodes is between 1900 and 2200°C. At this high operating temperature, contaminating electronegative

gases, which would increase the work function and reduce emission levels, are rapidly evaporated from the filament surface. As a result, tungsten filaments provide more stable gauge operation compared to metal oxide cathodes. The lifetime of *W* filaments, as determined by typical evaporation rates, is typically 1000 h at 10^{-6} torr. Tungsten is not seriously affected by hydrocarbons during operation.

Thoria-coated iridium (ThO_2Ir) filaments are the oxide-coated cathodes that are the most common filaments manufactured in the United States, whereas European filaments usually contain yttrium oxide instead. These cathodes are prepared by depositing a layer of thoria (i.e., thorium oxide) on a base metal of iridium by cataphoresis. Iridium is the preferred substrate because it is very resistant to oxidation and does not burn out if exposed to high air pressures while hot. ThO_2Ir filaments are very resistant to poisoning, and BA gauges with ThO_2Ir filaments are known to survive several brief exposures to atmospheric air without any performance deterioration.

The preferred material choice is dictated by application. Many of the material advantages are exhibited in the range outside the interest of electric propulsion testing (less than 10^{-8} torr or above 10^{-4} torr), and both are sufficient for electric propulsion testing.

III. Calibration

The National Institute of Standards and Technology (NIST) calibration for high vacuum (as low as 10^{-9} torr) uses a known gas that flows into the top of a vacuum chamber, passes through an orifice in the middle, and exits at the bottom. Kinetic theory allows the conductance of the orifice to be calculated from its known diameter, which in turn allows the pressure drop to be calculated accurately from the conductance and flow rate. Calibration by a gauge manufacturer is typically performed using an NIST reference spinning rotor gauge. A similar technique can be used during recalibration [22].

Calibration of the gauge should be performed with NIST traceability, with resulting uncertainties carried through the pressure measurement data reduction. The calibration should occur down to pressures at least one order of magnitude lower than expected during the range of testing.

With proper calibration, vendors specify accuracy with air better than $\pm 4\%$ and repeatability $\pm 3\%$. Testing has indicated an uncalibrated accuracy of 6% and, if calibrated on xenon, better than 3% accuracy. However, using the recommended gauge design and practices alone is still insufficient for accuracies better than $\pm 20\%$ without a quality controller. Experience using the Stabil-ion gauge without the controller also calibrated to NIST standards has shown comparable accuracies to standards BA gauges. The cabling, feedthrough lengths, and connector quality can also impact measurement accuracy. The recommended practice is that gauges should be calibrated to an NIST standard with the controller electronics, feedthrough and cabling, and gauge in the configuration to be used.

Numerous studies and past experience have also shown significant differences between gauges corrected for xenon when calibrated on air versus calibration on xenon [23]. It is a recommended practice that calibration should be performed on the primary gas of interest (e.g., xenon), if practical.

In general, the reproducibility of the hot-cathode gauges can be as good as 2% over a year of continuous operation in controlled vacuum conditions. A study of successive calibrations of 20 tube hot-cathode gauges with tungsten filaments showed the standard deviation of the maximum difference between successive calibrations was 3%, with a maximum of 12% [24]. The sensitivity of the gauges tended to decrease in most cases. The long-term stability of the pressure measurement is strongly affected by its operational history and gas exposure. Corrosive gases can quickly degrade the accuracy of BA gauges. Calibration intervals should be the lesser of 12 months or 2000 h of noncontinuous operation. Deviations from absolute accuracy with calibrated gauges is discussed in O'Hanlon [25].

IV. Setup and Measurement

Initial pumping of the facility should occur without operating the ionization gauge. The gauge may be turned on after the facility reaches less than or equal to 5×10^{-4} torr. The ionization gauge is typically mounted at the vacuum chamber wall. The assumption is that the distribution of particles everywhere in the chamber can be characterized, and thus measurement at one location is sufficient. For the base pressure, there are typically few pressure gradients. When the gas is flowing, pressure gradients must be understood. Modeling efforts are continuing to inform best practices for pressure measurements, including gauge locations, facility configuration influences, and methods for performing facility effect characterization [26].

A. Pressure Measurement and Gauge Location

The placement of the vacuum gauges greatly affects their uncertainty in measuring the background pressure. The uncertainty in vacuum pressure measurements arises from two sources: uncertainty inherent in the gauge, and varying pressure throughout the vacuum system. The uncertainty inherent in the vacuum gauge will usually be stated by the manufacturer and is unavoidable. The operating history of a hot-cathode gauge and the ambient environment in the vacuum system causes the gauge to act as either a source (outgassing) or sink (surface pumping) of gas. Typical 1 mA emission filaments require 10–15 W of input power. This amount of power is sufficient to cause thermal degassing from the gauge elements and surroundings. The significance of these effects depends on the characteristics of the vacuum system (i.e., a small ultrahigh vacuum system with low pumping speed is very sensitive to external sources and sinks of gas).

The second source of uncertainty comes from the pressure distribution in the chamber caused by localized placement of vacuum pumps and pumping surfaces. The pressure will be lower near the pumps. With an operating thruster, the pressure will also be high in the immediate vicinity of the discharge plume. Recommendations and requirements are provided to provide the highest pressure correlation to a relevant reference location with minimal uncertainty. In all cases, it is recommended to implement validated numerical models of the facility that can provide pressure data throughout the facility given pressure measurements at precise discreet locations.

Based on a large number of modeling efforts for multiple facilities and a range of thrusters, a few general recommendations for gauge placement are provided [5]. The pressure gauge should be mounted inside the vacuum chamber and have line of sight with the thruster. The pressure gauge should be mounted near the chamber wall at the exit plane of the thruster, located at least 0.6 chamber radii away from the centerline and at least 1 m from the outer diameter of the thruster. The pressure gauge can be standard flush mounted to the port but should not be mounted in a recessed cavity.

Limitations can make it impossible or inconvenient to mount the pressure gauge(s) along the wall at the exit plane. However, the pressure measurement should be reported as the pressure near the chamber wall at the exit plane of the thruster, and sufficient facility description and gauge location should be provided to allow the calculation of the pressure near the wall at the exit plane of the thruster. Additional uncertainties must be included due to the facility configuration, complexity of the geometries, distance from the exit plane, and method of calculating the pressure from the measurement location to the reference location.

If the pressure gauge cannot be located near the wall at the exit plane of the thruster, it should be located near the wall nearest the exit plane as practical, in front of the thruster, and before exposure to a 60 deg half-angle of the thruster channel wall nearest the gauge. The number of pumping surfaces between the exit plane of the thruster and the gauge should be minimized.

If the gauge(s) cannot be located downstream before exposure to the 60 deg half-angle, the gauge(s) should be at least 2 m downstream of the thruster exit plane. Additional shielding may be required as discussed previously when the gauge will be exposed to the plasma. The additional shielding and impact on measurements should be characterized (e.g., through a combination of both hot-fire and cold flow testing).

Pressure measurement should be made after the facility achieves steady state and no less than 2 min after a commanded flow-rate change greater than 10%. Commercial controllers have a typical

sampling rate of 60 Hz. The sampling rate should be no less than 10 Hz. To filter inherent noise, pressure should be measured as the 3 s average value.

It is recognized that pumping surfaces are often asymmetric near the thruster location due to facility design and limitations. Ideally, radial pumping asymmetry should occur at least 2 m downstream of the thruster, as far as is practical. However, because of conductance limitations, pumping surfaces are desired near the thruster exit plane.

Radial asymmetric pressure differentials should be minimized. Asymmetric pressure variation should be less than 20% at the thruster exit plane one thruster radius from the out exit channel wall. Performance, plume measurements, and life testing impacts of radial pressure asymmetries greater than 10% should be characterized based on specific test objectives.

B. Facility Effect Characterization

Because of limited data and relative low cost of augmenting electric propulsion testing, it is recommended that all future electric propulsion testing include background pressure effects characterization when practical. Baseline testing should occur at the maximum capability of the facility, and then measurements with the same diagnostics and methodology should be repeated with artificially increased background pressure. The background pressure range should encompass the background pressure expected over the life cycle of the thruster. Background pressure should be increased through supplemental supply of the primary gas (e.g., xenon) downstream of the thruster. There should be at least one pumping surface between the additional gas supply and the pressure gauge. The supplemental gas flow should be at least 2 m downstream of the thruster exit plane or preferably near the centerline of the facility. There is no absolute requirement on the position of the injected gas, provided that the environment is sufficiently characterized to discern pressure distribution and minimize differential pressure zones near the thruster and pressure gauge(s).

C. Calculations and Other Measurements

1. Reference Pressure

To support transportability of measurements in the literature, a pressure value should be provided to a common reference location. The relevant reference pressure should be near the wall at the exit plane of the thruster. The pressure should be corrected for the primary gas (e.g., xenon correction factor of 0.348). Although calibration and measurement using the gas of interest is preferred, a linear correction factor over the pressure range of interest is generally sufficient. Table 2 is a list of applicable correction factors.

If the measurement cannot be made directly, a calculation of the reference pressure is required. The reference pressure calculation can range from simple conductance and Clausing transmission corrections to high-fidelity facility pressure distribution simulations [27]. All assumptions necessary to independently reproduce the calculations should be recorded. Example calculations are provided in Sec. IV.D.

2. Neutral Density

Average neutral density can be obtained using the ideal gas law, where P is the pressure, n is the number density, k is Boltzmann's constant, and T is an average temperature. The temperature should be taken as the temperature of the chamber wall at the location of the pressure gauge.

Table 2 Common gas correction factors

Gas	Correction factor
Xe	0.348
Kr	0.515
Ar	0.775
H_2	2.17

3. Effective Pumping Speed

Facility pumping speeds are often reported based on the total additive capability of mechanical and cryogenic pumping systems. This method greatly exaggerates a facility's pumping capability, does not account for conductance losses, Clausing transmission limitations, or basic geometry/configuration impacts to pumping performance, and contributes to facility-to-facility comparison inconsistencies.

Facility pumping speed should be reported as the effective pumping speed at the exit plane of the thruster. Effective pumping speed should be calculated directly from the reference pressure calculation/measurement. This serves as a measurement of effective pumping speed. Assuming that the operating pressure is at least an order of magnitude greater than the base pressure, we can use Eq. (9):

$$p_{\text{Effective}} = \frac{\dot{m}}{p_{\text{measured}} - p_{\text{base}}} \tag{9}$$

The expected effective pumping speed can also be calculated using the vendor-specified performance but must include all performance losses from the pump to the facility (i.e., pump extension/nozzle, baffle, chevron, etc.) and facility losses. Rated pumping speeds also vary as a function of pressure and should be considered in facility calculations.

D. Example Calculations for Effective Pumping Speed

1. Effective Pumping Speed via Reference Pressure–Recommended Method

Assume that the facility base pressure was measured as 1×10^{-8} torr before thruster operation. A xenon thruster is being tested with a total (anode plus cathode) flow rate of 150 standard cubic centimeters per minute (sccm). The pressure near the wall at the exit plane of the thruster is measured as 1.3×10^{-5} torr. Determine the effective pumping speed of the facility at this set point.

First, convert the flow rate from sccm to torr liters per second·(l/s):

$$150\,\text{sccm} \times \frac{760\ \text{torr} \times 10^{-3}\ \text{l}/60\ \text{s}}{1\,\text{sccm}} = 1.9\frac{\text{Torr l}}{\text{s}} \tag{10}$$

Then, applying Eq. (9):

$$P_{\text{Effective}} = \frac{1.9\ \text{Torr l/s}}{1.3 \times 10^{-5}\ \text{Torr} - 1.0 \times 10^{-8}\ \text{Torr}} = 150{,}000\ \text{l/s} \tag{11}$$

Note that if the pressure gauge was calibrated for air, the xenon correction factor is 2.87. Therefore, the corrected pressure reading would be 4.54×10^{-6} torr, and then applying Eq. (9) would yield 420,000 l/s.

2. Effective Pumping Speed via Facility Description–Oil Diffusion Pump Facility

To illustrate the procedure for calculating the effective pumping speed at any location in a facility through description, NASA Glenn Research Center (GRC) Vacuum Facility (VF) 7 is used. NASA GRC's VF-7 is a 10 ft diameter × 15 ft length facility with a historical base pressure of 1×10^{-7} torr and rated with a nominal pumping speed of 115,000 l/s (air) using five 32 in. oil diffusion pumps (ODPs). The facility schematic and pump locations are illustrated in Fig. 5. For calculations, the radius of the facility is 59.5 in. for an area of 11,122 in.^{2} (71,754.8 cm^2). The length of the facility is 118 in. with ODP 1, ODPs 2 and 3, and ODPs 4 and 5 located at 37.5, 96.0, and 154.5 in., respectively.

Most facilities of interest have a cylindrical shell design. Calculations for conductance in a pipe are straightforward and often used. However, the pipe equation yields its best accuracy when the length-to-diameter (L/D) ratio is greater than 10, whereas most facilities have L/D ratios less than 5. To accommodate this lower ratio, it is recommended to calculate aperture conductance and then apply the Clausing transmission coefficient for the length-to-diameter component [26]. Molecular conductance is provided in Eq. (12):

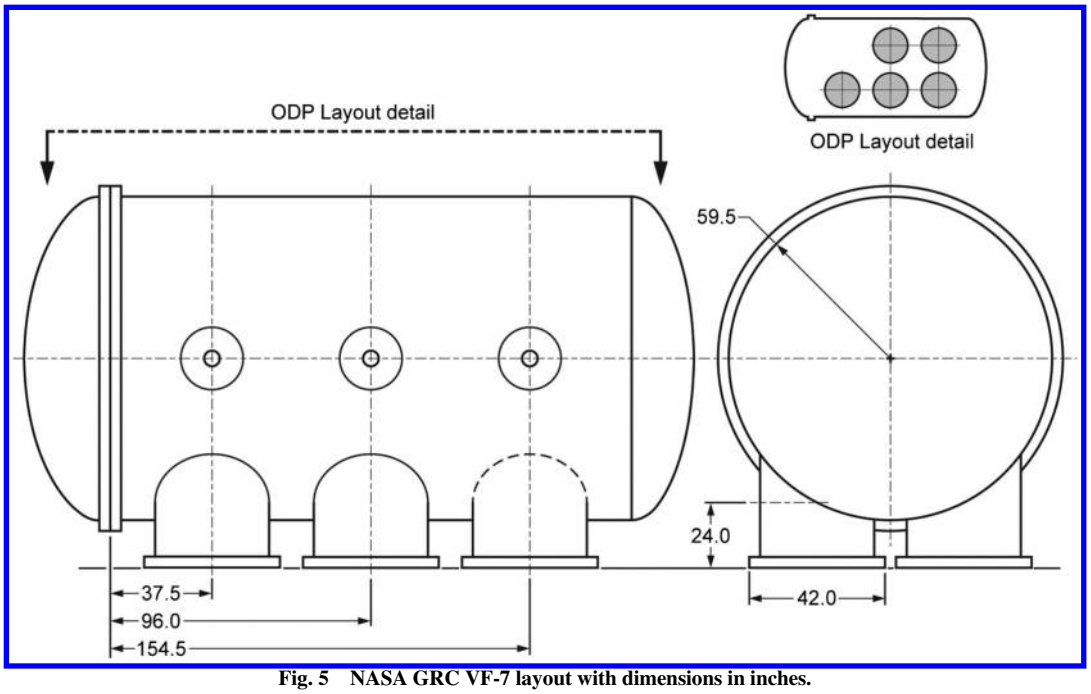

Fig. 5 NASA GRC VF-7 layout with dimensions in inches.

$$C_M = I_R\, a\, A \tag{12}$$

Clausing transmission coefficients are dependent on the length-to-radius ratio, as shown in Fig. 6. The solution to the Clausing integral provides the transmission probability that a molecule will pass from one end of the pipe to exit the other end.

The flow rate across the aperture is dependent on gas species because molecular velocities are dependent on molecular weight. A molecular impact rate is established for specific gas species using the following equation [26]:

$$I_R = P \times 3.5 \times 10^{22}/(M \times T)^{1/2} \tag{13}$$

Calculations included here are for air and xenon because they are the most relevant to provided pump data and standard Hall and gridded-ion operation, respectively. The base pressure used is dependent on the base pressure of the particular chamber recorded during testing with no propellant flow. A typical ODP installation will have a circular extension/nozzle extending from the main vessel terminating with a flange for bolting. The conductance for this nozzle will determine the delivered pumping capability to the main chamber. As required by International Standards Organization (ISO) Standard 1608 [28], the gauge tube is mounted at $D/2$ above the connecting flange of the pump, and for American Vacuum Society (AVS) 4.1 [29], the mounting distance is $D/4$. The gauge location, as measured from the chamber flange, will be subtracted from the overall length of the nozzle when calculating the conductance.

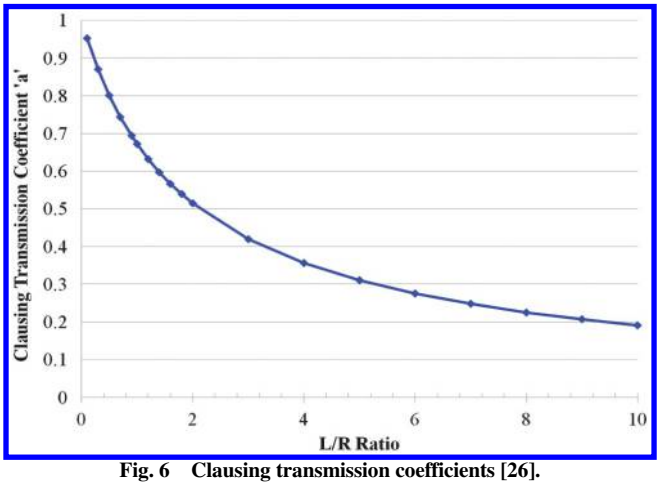

Fig. 6 Clausing transmission coefficients [26].

The nozzle extension houses a chevron baffle directly above the ODP, or in some cases the chevron is bolted directly to the ODP. If the conductance of the chevron is provided by the manufacturer, then the pumping speed at the chevron outlet can be found using Eq. (14):

$$1/P_{\text{Eff}} = 1/P_S + 1/C_{\text{Baffle}} \tag{14}$$

Because the baffle is not mounted at the gauge distances listed in either ISO 1608 or AVS 4.1, an equivalent pump speed at the opening of the pump is necessary for the calculation. Again, we use the Clausing transmission coefficient to find the equivalent pump speed. For $D/2$ (R) and $D/4(R/2)$, the coefficients are 0.672 and 0.801, respectively. For VF-7, the ISO speeds are rated for air at 23,000 l/s mounted according to ISO 1608; therefore, the equivalent speed at the pump entrance is given by Eq. (15):

$$P_{\text{Eq}} = P_S/a = (23{,}000\ \text{l/s})/0.672 = 34{,}230\ \text{l/s} \tag{15}$$

It is also common practice for the baffle manufacturers to provide a pumping speed reduction factor k. For VF-7, the chevron manufacturer provided a correction factor of 50%. This can be used to determine the conductance of the baffle:

$$P_{\text{Eff}} = kP_{\text{Eq}} \tag{16}$$

$$1/(kP_{\text{Eq}}) = 1/P_{\text{Eq}} + 1/C_{\text{Baffle}} \tag{17}$$

Therefore,

$$C_{\text{Baffle}} = kP_{\text{Eq}}/(1-k) \tag{18}$$

For the chevron,

$$C_{\text{Chevron}} = 0.5 \times 34{,}230\text{l/s}/(1-0.5) = 34{,}230\ \text{l/s (air)} \tag{19}$$

The halo baffle manufacturer provides a correction factor of 60%.

For the halo baffle,

$$C_{\text{Baffle}} = 0.6 \times 34{,}230 \text{ l/s}/(1 - 0.6) = 51{,}530 \text{ l/s (air)} \quad (20)$$

The example chamber has a 24 in. nozzle length and a 42 in. nozzle diameter, yielding a Clausing coefficient of 0.644. The conductance of the nozzle is given by Eq. (21):

$$C_{\text{Nozzle}} = V A a \quad (21)$$

The volumetric flow rate can be found using the perfect gas equation and surface impact calculations provided in Eqs. (22), and (23), respectively:

$$PV = nRT \quad (22)$$

$$I_S = 3.5 \times 10^{22} \times P/(M \times T)^{1/2} \quad (23)$$

Assuming a temperature of 293 K, M for air and xenon as 28.96 and 131.29, respectively, and the measured base pressure of 3×10^{-7} torr:

$$\text{IS(Air)} = 3.5 \times 1022 \cdot 3 \times 10 - 7/(28.96 \cdot 293)\frac{1}{2} = 1.1399 \times 1014 \text{ atoms}/(\text{cm}^2 \cdot \text{s}) \quad (24)$$

$$\text{IS(Xe)} = 3.5 \times 1022 \cdot 3 \times 10 - 7/(131.29 \cdot 293)\frac{1}{2} = 5.3535 \times 1013 \text{ atoms}/(\text{cm}^2 \cdot \text{s}) \quad (25)$$

The impact rate is used to find the volumetric flow rate by substituting into the ideal gas equation where n is equal to the impact rate divided by Avogadro's number to convert particles into moles yielding Eq. (26):

$$V = (I_S/6.022 \times 10^{23}) \cdot R \cdot T/P \quad (26)$$

yielding

$$V = 11.529 \text{ l/cm}^2 \cdot \text{s (Air)} \quad \text{and} \quad 5.415 \text{ l/cm}^2 \cdot \text{s (Xe)} \quad (27)$$

Finally, substituting into Eq. (21) for Xe:

$$C_{\text{Nozzle}} = 11.529 \cdot 8938 \cdot 0.643587 = 66{,}322 \text{ l/s(Air)} \quad (28)$$

The system conductance for the single ODP at the vessel entrance is

$$1/C_{\text{Total}} = 1/C_{\text{Chevron}} + 1/C_{\text{Baffle}} + 1/C_{\text{Nozzle}} \quad (29)$$

Therefore,

$$C_{\text{Total}} = 1/(1/51{,}341 + 1/34{,}227 + 1/66{,}337) = 15{,}681 \text{ l/s (Air)} \quad (30)$$

Using the effective pumping speed and nozzle conductance, the pumping speed at the entrance to the chamber can be calculated as

$$1/P_{\text{Entrance}} = 1/P_{\text{Eff}} + 1/C_{\text{Total}} \quad (31)$$

Therefore,

$$P_{\text{Entrance}} = 10{,}754 \text{ l/s(Air)} \quad \text{and} \quad 5058 \text{ l/s (Xe)} \quad (32)$$

From these calculations, we can predict what gauges should read from various locations in the chamber using superposition of each of the pumps individual speeds with respect to the conductance calculated for the distance to the pump. Assume that the thruster is located 50 cm (~20 in.) from the end cap and thrusting into the chamber at a location before the plane of the first pumping surface, as is often the case. The distances from pump 1, pumps 2 and 3, and pumps 4 and 5 from the chamber entrance in combination with the radius of the facility provide the Clausing coefficients of 0.76, 0.56, and 0.45, respectively. Equation (1) is then applied to calculate the conductance and then finally effective pumping from each of the pumps and summed for the total effective pumping speed, as shown in Eqs. (33), and (34):

$$P_{\text{Eff}}(\text{Pump 1}) = 1/(1/C + 1/P_{\text{Entrance}}) = 1/(1/297{,}279 + 1/5058) = 4973 \text{ l/s (Xe)} \quad (33)$$

$$P_{\text{Eff}}(\text{Pumps 2 and 3}) = 1/(1/219{,}831 + 1/10{,}117) = 9672 \text{ l/s (Xe)} \quad (34)$$

$$P_{\text{Eff}}(\text{Pumps 4 and 5}) = 1/(1/178{,}324 + 1/10{,}117) = 9574 \text{ l/s (Xe)} \quad (35)$$

Then, by superposition,

$$P_{\text{Total}} = 24{,}219 \text{ l/s (Xe)} \quad (36)$$

This methodology can be applied to calculate the effective pumping speed from anywhere in the chamber. A plot of effective pumping speed throughout the facility is shown in Fig. 7. Note that the effective pumping speed is significantly different from the basic sum of the individual pumps. Also, the highest effective pumping speed is achieved by placing the thruster with the exit plane directly over the middle two ODPs. The calculations for individual pump contributions are provided in Table 3 as a function of distance from the end cap.

Verification of the approach was achieved by performing flow testing with xenon. BA gauges were placed on facility ports for testing over a range of flow rates. During the testing, the base pressure was 9.7×10^{-7} torr. The data from the gauge located 96.0 in. (243.8 cm) from the end cap are shown in Table 4. All of the calculated pressures matched the measured pressure within the uncertainty range of the pressure gauge.

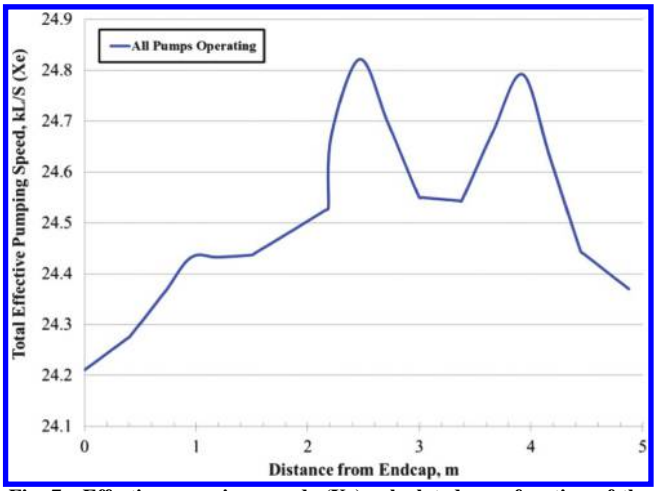

Fig. 7 Effective pumping speeds (Xe) calculated as a function of the location.

Table 3 Individual pump contributions (l/s Xe) and their totals referenced to chamber location

Distance, in.	ODP 1	ODPs 2 and 3	ODPs 4 and 5	Total
0.0	4973	9,672	9,574	24,219
12.0	5021	9,694	9,594	24,309
24.0	5024	9,717	9,613	24,354
37.5	5058	9,742	9,634	24,434
49.5	5015	9,766	9,656	24,437
61.5	5012	9,790	9,678	24,480
73.5	5009	9,814	9,700	24,523
85.5	5006	9,839	9,722	24,568
96.0	5004	10,117	9,742	24,863
108.0	5001	9,836	9,766	24,603
120.0	4998	9,811	9,790	24,600
132.0	4996	9,811	9,790	24,598
144.0	4994	9,763	9,839	24,596
154.5	4991	9,742	10,117	24,851
166.5	4989	9,719	9,836	24,544
178.5	4985	9,697	9,811	24,494
192.0	4983	9,672	9,784	24,439

Table 4 Comparison of calculated to measured pressure readings

Xenon flow, sccm	Pressure predicted, torr	Corrected pressure measured, torr	(Predicted — measured) / measured, %
20	1.12×10^{-5}	1.09×10^{-5}	2.5
40	2.14×10^{-5}	2.21×10^{-5}	−3.3
50	2.65×10^{-5}	2.70×10^{-5}	−1.9
60	3.16×10^{-5}	3.22×10^{-5}	−1.9
67	3.52×10^{-5}	3.50×10^{-5}	0.4

3. *Effective Pumping Speed via Facility Description with Cryogenic Pumping*

Cryogenic pumps can be added as either an external pumping port or as an internal paneled array. For pumps mounted to the side port of the main chamber, the procedure for assessing the nozzle inlet conductance and effective pump speed is the same as for the oil diffusion pump. In the case of the internal pumping panels, the cross-sectional area of the panel is an obstruction to the molecular flow and must be subtracted from chamber cross section for an equivalent diameter. An example is the NASA GRC VF-5 with 10 pairs of oil diffusion pumps, as shown in Fig. 8. Using the same methodology as before for ODPs, the effective pumping speed can be calculated over the length of the facility. Starting farthest from the cryogenic panels, the effective pumping speed of the first pair of ODPs is shown in Fig. 9. The figure illustrates that the effective pumping speeds peak directly over the pumps and decrease significantly downstream where the cryogenic panels limit the pumping conductance cross-sectional area.

The two vertical cryogenic panels are 280 by 300 cm, and there are four horizontal panels 140 by 457 cm. The panels can pump from front and back surfaces. Using their average pumping speed value, it would indicate a total pumping speed of 4,840,000 l/s (air). However this cannot be achieved because the total conductance of the 457 cm equivalent diameter chamber is only 1,890,200 l/s. The horizontal panels overlap reducing their efficiency to 80%. Using the effective pumping speed calculation, the maximum pumping speed is calculated to be 1,310,000 l/s (air). Therefore, the ODPs located under the cryogenic panels are in a region that is already being pumped at the maximum of the shell conductance, and their contribution to the pumping speed of the facility is not evident. This results in a constant pumping speed in the cryogenic pumping region of 1,310,000 l/s (air). The effective pumping speed of the entire facility is shown in Fig. 10.

As with VF-7, the calculation methodology was tested to compare predicted versus measured pressures. For VF-7, the base pressure was 8.0×10^{-7} torr before flow testing. Sample results are provided in Table 5.

4. *Temperature-Correction Methodology*

Under typical room-temperature operating conditions, temperature effects are negligible. However, temperature effects cannot be ignored when gauges are used at or attached to chambers at a wide range of temperatures [30]. The gauge ion current is directly proportional to the neutral density within the gauge:

$$n_{\text{gauge}} \sqrt{T_{\text{gauge}}} = n_{\text{chamber}} \sqrt{T_{\text{chamber}}} \tag{37}$$

The gauge sensitivity factor during calibration is determined:

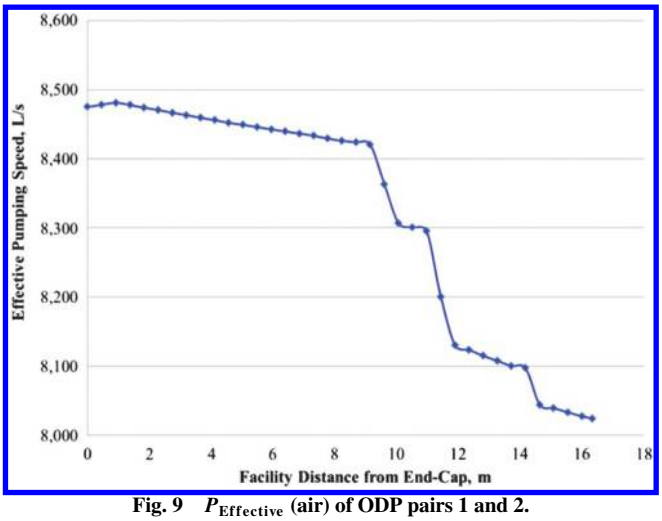

Fig. 9 $P_{\text{Effective}}$ (air) of ODP pairs 1 and 2.

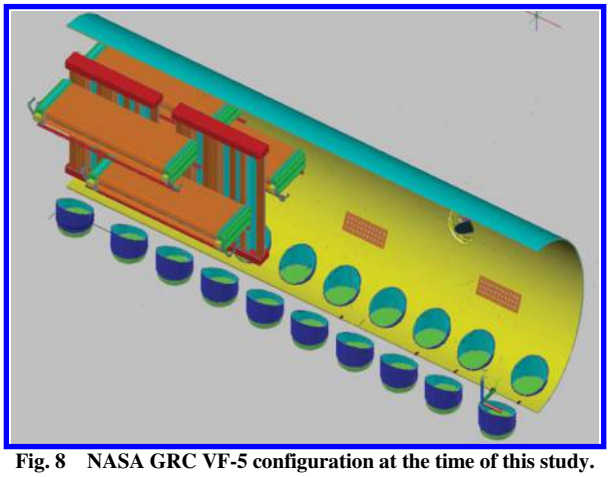

Fig. 8 NASA GRC VF-5 configuration at the time of this study.

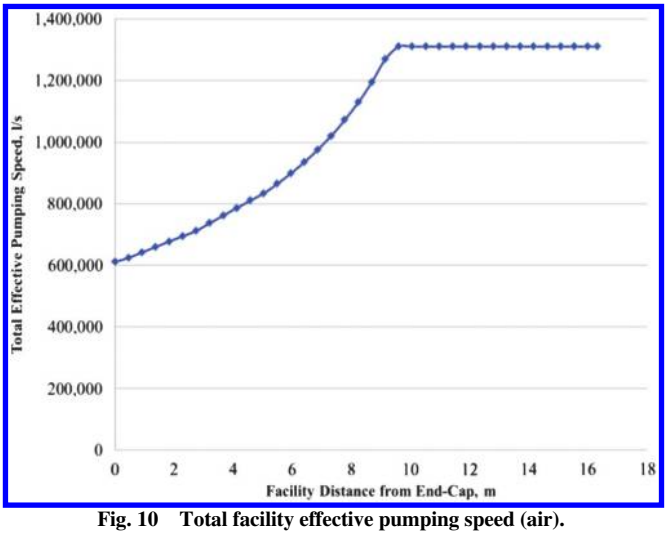

Fig. 10 Total facility effective pumping speed (air).

Table 5 Comparison of calculated to measured pressure readings

Xenon flow, sccm	Pressure predicted, torr	Corrected pressure measured, torr	(Predicted — measured) / measured, %
405	1.92×10^{-5}	2.20×10^{-5}	−12.7
613	2.87×10^{-5}	3.00×10^{-5}	−4.5
838	3.89×10^{-5}	3.80×10^{-5}	2.3

$$S_{n_{\text{gauge}}} = \frac{I_c}{n_{\text{gauge}}} = \frac{I_c}{n_{\text{chamber}}}\sqrt{\frac{T_{\text{gauge}}}{T_{\text{chamber}}}} \tag{38}$$

If the temperature of the gauge is not measured and a gauge-sensitivity constant is used, it is related to the gauge sensitivity by

$$S_{n_{\text{chamber}}} = S_{n_{\text{gauge}}}\sqrt{\frac{T_{\text{chamber}}}{T_{\text{gauge}}}} \tag{39}$$

If the gauge temperature at calibration is unknown, then the chamber sensitivity constant is not a true constant, and it is not possible to determine the gauge sensitivity factor. As shown earlier, if the gas temperature is in a range where condensation does not occur, the gauge sensitivity is independent of temperature, and current is only dependent on the neutral density. However, the neutral density in the gauge will depend on temperature of the gauge and the chamber:

$$n_{\text{chamber}} = \frac{I}{S_{n_{\text{gauge}}}}\sqrt{\frac{T_{\text{gauge}}}{T_{\text{chamber}}}} \tag{40}$$

If a gauge is calibrated in terms of pressure in the gauge envelope,

$$P_{\text{gauge}} = n_{\text{gauge}} k T_{\text{gauge}} \tag{41}$$

Using the relationship that

$$S_{P_{\text{gauge}}} = \frac{I_c}{P_{\text{gauge}}} \tag{42}$$

then

$$S_{P_{\text{gauge}}} = \frac{I_c}{n_{\text{gauge}} k T_{\text{gauge}}} = \frac{S_{n_{\text{gauge}}}}{k T_{\text{gauge}}} \tag{43}$$

If a gauge is calibrated using pressure in the calibration chamber with a known calibration temperature,

$$I_c = S_{P_{\text{chamber}}} P_{\text{chamber}} = S_{P_{\text{chamber}}} n_{\text{chamber}} k T_{\text{chamber}} \tag{44}$$

and

$$S_{P_{\text{chamber}}} = \frac{S_{n_{\text{gauge}}}}{k T_{\text{chamber}}}\frac{n_{\text{gauge}}}{n_{\text{chamber}}} = \frac{S_{n_{\text{gauge}}}}{k T_{\text{chamber}}}\sqrt{\frac{T_{\text{chamber}}}{T_{\text{gauge}}}} \tag{45}$$

resulting in the final correction factor shown in Eq. (46):

$$S_{P_{\text{chamber}}} = S_{P_{\text{gauge}}}\sqrt{\frac{T_{\text{gauge}}}{T_{\text{chamber}}}} \tag{46}$$

Using these relationships, it is now possible to determine temperature-correction factors for gauge pressure indications. Correction must be made to the gauge "indicated" pressure shown by the controller. Therefore, the true chamber pressure, with measured temperatures of the gauge and chamber:

$$P_{\text{truth}} = n_{\text{truth}} k T_{\text{truth}} = n_{\text{gauge}e_{\text{measured}}} k \sqrt{T_{\text{gauge}e_{\text{measured}}} T_{\text{chamber}_{\text{measured}}}} \tag{47}$$

then using our relationships and substitution:

$$P_{\text{truth}} = P_{\text{indicated}}\sqrt{\frac{T_{\text{gauge}e_{\text{measured}}} T_{\text{chamber}_{\text{measured}}}}{T_{\text{gauge}e_{\text{calibration}}} T_{\text{chamber}_{\text{calibration}}}}} \tag{48}$$

Example 1: Consider a gauge at room temperature (300 K), calibrated at room temperature (300 K), and attached to a liquid nitrogen-cooled chamber (77 K):

$$P_{\text{truth}} = P_{\text{indicated}}\sqrt{\frac{300 \cdot 77}{300 \cdot 300}} = 0.506 \cdot P_{\text{indicated}} \tag{49}$$

Example 2: Consider a gauge calibrated at room temperature (300 K), held at liquid nitrogen temperature (77 K) and attached to a liquid nitrogen-cooled chamber (77 K):

$$P_{\text{truth}} = P_{\text{indicated}}\sqrt{\frac{77 \cdot 77}{300 \cdot 300}} = 0.257 \cdot P_{\text{indicated}} \tag{50}$$

V. Pressure Requirements

Facility effects impact various measurements differently. Performance is primarily affected by ingested propellant background gas, which can be difficult to estimate. Lifetime is primarily affected by the changes in the ion fluxes that cause erosion of the various thruster surfaces. Far-field plume measurements are most sensitive to fluctuations in the plasma densities and energies caused by the facility environment. Early testing of the Stationary Plasma Thruster (SPT)-100 provided guidance regarding acceptable facility pressure requirements for performance and near-field plume measurements: 5×10^{-5} and 1.3×10^{-5} torr, respectively and residual gas background pressures below 5×10^{-6} torr [31,32]. The authors note that the basis for this guidance does not include any specifications regarding pressure measurement methodology, locations, correction factors, or even the applicability to thrusters beyond the SPT-100.

Extremely low levels of contaminants can have profound effects on measured lifetimes. Nitrogen and air can interact with surfaces and drastically change their sputter rates. Also, there are limited data on background partial pressures. For gridded ion engines, it has been observed that breakdown rates of ion thruster begins to be affected in the low 10^{-5} torr range, and lifetime measurements may be impacted at 5×10^{-7} torr of contaminant partial pressures [33]. With the NSTAR life test conducted at 4×10^{-6} torr and nominal flight mission performance, it is likely to become the accepted standard for life testing of gridded-ion engines [34]. The NEXT Long Duration Test has been conducted at a maximum pressure of 2.5×10^{-6} torr [35], and the BPT-4000 Life Test was conducted at 2.5×10^{-5} torr.

Several past studies have highlighted thruster performance and various diagnostic measurement sensitivities to facility background pressure [36]. Analysis and testing of the specific thruster should be performed to understand the impact of facility pressure on in-space performance and life. However, there are insufficient test data for absolute requirements for all thruster designs, scales, and measurements of interest. Hall thrusters in particular have sparse data in the open literature with potentially high dependence on background pressure to design and performance.

A recent investigation of transportability of electric propulsion measurements and dependence on background pressure of the SPT-100 Hall thruster was conducted [37]. The investigation included the use of a Stabil-ion gauge. The tests were conducted at two disparate facilities, but the pressure gauges were placed in approximately the same location relative to the thruster. The goal of testing is to

sufficiently predict performance during application. The tests indicated that background pressures below 1×10^{-5} torr were necessary to identify the sharp change in the slope of thrust measurements between 3×10^{-5} and 0 torr. The slopes for both efficiency and specific impulse approach linearity in the range of $2 - 3 \times 10^{-5}$ torr. The testing extrapolated to a fractional 13.8% change in efficiency from 5×10^{-5} and 0 torr. The current utilization efficiencies derived from Langmuir probe and Retarding Potential Analyzer (RPA) measurements appear to level off below 2×10^{-5} torr. Finally, discharge current stability, breathing mode frequency, plasma potential, electron temperature, and densities continue to change well into the 10^{-6} torr range. The results show that making accurate pressure measurements traced to a common reference does allow transportability of results across facilities. However, the results alone are insufficient to justify a set of absolute pressure requirements for general thruster designs. Until absolute pressure standards can be justified for categories or general designs of thrusters, future qualification programs will need to determine the maximum operating pressure that can be used to reliably correlate ground-test data with space operation.

VI. Cautionary Notes

A. Correlation to Reference

The most critical concern with pressure measurements and effective pumping speeds is the proper correlation to the reference plane and sources of discrepancies. Consider a 60-ft-long facility with a 15 ft diameter, with the far end cap open to space (i.e., infinite pumping capability). Regardless of pumping capability, the facility has a maximum conductance of 889,000 l/s. Placing the thruster 1 m from the near wall and pressure gauges at two different locations highlights the importance of conductance and the need to correlate to the reference plane.

Testing a moderate 4.5 kW thruster is this configuration, with infinite pumping speed, will not meet the required background pressure for performance testing. Also, the two wall gauges, if used directly, would indicate that the facility does have sufficient performance, shown in Fig. 11. Most importantly, either gauge, if correlated correctly, could be used to calculate the reference pressure and effective pumping speed. The emphasis is not on limitations of where measurements are performed, rather that they are correlated to an appropriate and relevant reference. In this example case, Fig. 11 is modeled using the Hypersonic Aerothermodynamics Particle code [38] to perform three-dimensional direct simulation Monte Carlo simulations of facility pressure distributions.

B. Gauge History Dependence

The dependence of the sensitivity drifts on the type of gauge and its operating conditions has made it impossible to develop a unified model or theory that completely and systematically explains all experimental observations. Most knowledge is phenomenological and based on the experience accumulated over several decades of pressure measurements with commercial BA gauges.

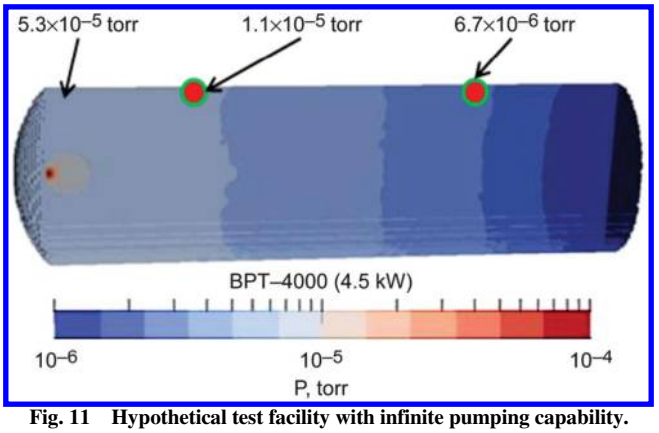

Fig. 11 Hypothetical test facility with infinite pumping capability.

Instabilities in commercial ionization gauges can often be traced back to changes in the path of the electron beam caused by several different aging effects [39]. Most ion gauge controllers do an adequate job at maintaining the electron emission current and bias voltages at a constant value; however, they have no influence over the trajectories of the electrons once they leave the hot filament surface.

Changes in the emission characteristics of the filament are of high concern because they directly affect the electron trajectories and can result in changes in both the potential distribution and the charged particle trajectories inside the anode grid [40]. Large variations in the emission characteristics of the filament can be caused by the following effects [6].

1. Changes in Geometry of the Electrode Structure

This effect is often due to either repeated thermal cycling and/or mechanical shock and can be mitigated through the use of tensioned filaments and electrode supports.

2. Local Temperature Induced Degradation

Filaments will degrade over time and exhibit continuous metal evaporation during emission, thinning the filament. The filament is usually the life-limiting element of a BA gauge. As the filament becomes thinner, the controller will increase the filament temperature to maintain current with the reduced surface area [41]. Preferential depletion of the central portion of the filament will cause changes in the filament shape and temperature distribution, resulting in a change in electron emission distribution along the filament. The filament should be visually inspected during each calibration cycle.

3. Surface Contamination and Chemical Reaction

Surface contamination with impurity diffusion can change both the emissivity of the cathode surface and the work function. Also, cathode poisoning from repeated exposure to air and humidity may increase the work function of the filament, impacting the operating temperature of the gauge.

4. Changes in the Filament Coating

Many cathodes have deposits of low-work-function layers on refractory metal wires with potential to degrade or detach during use. Evaporation and ion bombardment may also deplete the central portion of the coating, resulting in differential emission shifting toward the ends of the filament.

C. Leakage Currents

Hot-cathode ionization gauges operate through the collection of small currents, and therefore leakage currents can significantly impact performance and should be mitigated. Leakage current may occur around the electrical connection to the gauge pins. Plasma electrons can enter in the gap between the plug and gauge and affect measurements. To prevent this leakage current, the connection point should be covered in an insulating tape. The area around the collector pin on the gauge must be kept clean at all times on both the air and vacuum sides of the feedthrough connectors. It is important to have quality leads to make good connections to the controller.

D. Outgassing

The outgassing of hot-cathode gauges is a potentially large source of error when such gauges are used at base pressure levels in high vacuum systems. Outgassing levels are particularly high when a gauge is turned on for the first time after exposure to ambient or high gas pressures. Degassing and/or bakeout can reduce the outgassing during testing. The recommended method to reduce gauge outgassing is to bake out the gauge for an extended period of time. BA gauges are typically degassed after the gauge has been exposed to ambient or if surface contamination is suspected. The BA gauge should not be used for at least 1 h after degassing, but multiple hours are preferred.

The NIST High Vacuum Group, concerned mostly with pressure ranges near electric propulsion base pressures and below, recommends

the elimination of the degassing practice. Observations have shown that gauges effectively degas during normal operation while the vacuum system is baked. Their recommendation is to only degas if the gauge is heavily contaminated or after exposure to active gases such as oxygen and to degas at the minimum current for a longer period of time [42]. Modern controllers allow for degas power and time variability.

VII. Conclusions

Facility background pressure is known to impact the performance, internal thruster environments, near-field plume measurements, etc. Various thrusters and designs have shown inconsistent trends in diagnostic measurements due to background pressure. Thrusters are tested at various facilities and conditions throughout research, development, qualification, system integration, and mission operations. The community currently lacks sufficient test data and analyses to analytically correct for all facility effects. The literature archives include significant test efforts without pressure measurements provided at a relevant reference or sufficient information to calculate independently. Existing practices rely on gauges known to have inaccuracies several factors higher than achievable with proper hot-cathode gauge construction, NIST controllers, and calibration. Without community consensus on pressure requirements, it is difficult to advocate for facility investments, or worse, inconsistencies may question the validity of key results from costly tests. This paper is only a preliminary step toward pressure measurement standardization, and it is greatly anticipated that the community will continue additional testing to help refine and define additional pressure requirements and facility effect characterization. Rigorous additional testing and analyses are required to establish formal pressure testing requirements and standards. It is critical to the community to develop standardization that allows transportability of data between facilities but especially that allows it to correlate ground-test data to flight system performance. Following consistent test practices with pressure referenced to a common location has been demonstrated to effectively permit transportability of data. This paper serves as a starting point with initial recommendations on electric propulsion test practices relative to pressure measurements based on contemporary knowledge of facility effects until more rigorous efforts can be completed.

Acknowledgments

The work described in this paper was funded in part by the In-Space Propulsion Technology Program, which is managed by NASA's Science Mission Directorate in Washington, D.C., and implemented by the In-Space Propulsion Technology Project at the John Glenn Research Center in Cleveland, Ohio.

References

[1] Blott, R., Robinson, D., and Gabriel, S., "Verification—Electric Propulsion's Achilles Heel," *Proceedings of the 32nd International Electric Propulsion Conference*, IEPC-2011-061, Wiesbaden, Germany, Sept. 2011, http://erps.spacegrant.org/.

[2] Blott, R., Robinson, D., and Gabriel, S., "Electric Propulsion Verification—Managing Measurement Uncertainty," *63rd International Astronautical Congress*, IAC-12-C4.4.9x13215, Naples, Italy, Oct. 2012.

[3] deGrys, K., Mathers, A., Welander, B., and Khayms, V., "Demonstration of 10,400 Hours of Operation on a 4.5 kW Qualification Model Hall Thruster," *46th AIAA/ASME/SAE/ASEE Joint Propulsion Conference and Exhibit*, AIAA Paper 2010-6698, July 2010.

[4] Byers, D., and Dankanich, J. W., "A Review of Facility Effects on Hall Effect Thrusters," *Proceedings of the 31st International Electric Propulsion Conference*, IEPC-2009-076, Ann Arbor, MI, Sept. 2009.

[5] Dankanich, J. W., Swiatek, M. W., and Yim, J. T., "A Step Towards Electric Propulsion Testing Standards: Pressure Measurements and Effective Pumping Speeds," *48th AIAA/ASME/SAE/ASEE Joint Propulsion Conference & Exhibit*, AIAA Paper 2012-3737, July 2012.

[6] "IGC100 Ion Gauge Controller: Appendix A: Bayard–Alpert Ionization Gauges," *Standard Research Systems*, 2012.

[7] "Granville-Phillips Series 370 Stabil-Ion Vacuum Gauge and Controller," MKS Instruments Document No. 141607-EN-US, Rev. D., Dec. 2014.

[8] "Bayard–Alpert Ionization Gauges," *Stanford Research Systems*, 2012.

[9] Tilford, C. R., "Pressure and Vacuum Measurements," *Determination of Thermodynamic Properties*, 2nd ed., edited by Rossiter, B. W., and Baetzold, R. C., Vol. 6, Physical Methods of Chemistry, Wiley, New York, 1992, pp. 101–173.

[10] Filipelli, A., and Dittmann, S., "Search for Pressure Dependence in the Sensitivity of Several Common Types of Hot-Cathode Ionization Gauges for Total Pressures Down to 10^{-7} Pa," *Journal of Vacuum Science & Technology A*, Vol. 9, No. 5, 1991, pp. 2757–2765.

[11] "Gas Correction Factors for Bayard–Alpert Ionization Gauges," Stanford Research Systems, http://www.thinksrs.com/downloads/PDFs/ApplicationNotes/IG1BAgasapp.pdf.

[12] Kauert, R., Kieler, O., Biehl, S., Knapp, W., Edelmann, C., and Wilfert, S., "Numerical Investigations of Hot Cathode Ionization Gauges," *Vacuum*, Vol. 51, No. 1, Sept. 1998, pp. 53–59.

[13] Alpert, D., "New Developments in the Production and Measurement of Ultra High Vacuum," *Journal of Applied Physics*, Vol. 24, No. 7, 1953, pp. 860–879.

[14] Szwemin, P. J., "The Influence of External Circuit on the Ionization Gauge Stability," *Vacuum*, Vol. 41, Nos. 7–9, 1990, pp. 1807–1809.

[15] Donkov, N., and Knapp, W., "Control of Hot-Filament Ionization Gauge Emission Current: Mathematical Model and Model-Based Controller," *Measurement Science and Technology*, Vol. 8, No. 7, 1997, pp. 798–803.

[16] Tilford, C. R., "Reliability of High Vacuum Measurements," *Journal of Vacuum Science & Technology A*, Vol. 1, No. 2, 1983, pp. 152–162.

[17] Close, K. J., Lane, D., and Yarwood, J., "Thermal Effects on Hot-Cathode Ionization Gauges," *Vacuum*, Vol. 29, No. 7, 1979, pp. 249–250.

[18] Dushman, S., and Lafferty, J. M., *Scientific Foundations of Vacuum Technique*, 2nd ed., John Wiley & Sons, Inc., 1962.

[19] Arnold, P. C., and Borichevsky, S. C., "Nonstable Behavior of Widely Used Ionization Gauges," *Journal of Vacuum Science & Technology A*, Vol. 12, No. 2, 1994, pp. 568–573.

[20] Arnold, P. C., Bills, D. G., Borenstein, M. D., and Borichevsky, S. C., "Stable and Reproducible Bayard–Alpert Ionization Gauge," *Journal of Vacuum Science & Technology A*, Vol. 12, No. 2, 1994, pp. 580–586.

[21] Filippelli, A. R., "Influence of Envelope Geometry on the Sensitivity of Nude Ionization Gauges," *Journal of Vacuum Science & Technology A*, Vol. 14, No. 5, 1996, pp. 2953–2957.

[22] Dittmann, S., "NIST Measurement Services: High Vacuum Standard and Its Use," National Inst. of Standards and Technology Special Publ. 250-34, Gathersburg, MD, March 1989.

[23] Garner, C. E., Tverdokhlebov, S. O., Semenkin, A. V., and Garkusha, V. I., "Evaluation of a 4.5-kW D-100 Thruster with Anode Layer," *32nd Joint Propulsion Conference and Exhibit*, AIAA Paper 1996-2967, July 1996.

[24] Filippelli, A. R., and Abbott, P. J., "Long-Term Stability of Bayard–Alpert Gauge Performance: Results Obtained from Repeated Calibrations Against the National Institute of Standards and Technology Primary Vacuum Standard," *Journal of Vacuum Science & Technology A*, Vol. 13, June 1995, pp. 2582–2586.

[25] O'Hanlon, J. F., *A User's Guide to Vacuum Technology*, 3rd ed., Wiley, Hoboken, NJ, 2003.

[26] Yim, J. T., and Burt, J. M., "Characterization of Vacuum Facility Background Gas Through Simulation and Considerations for Electric Propulsion Ground Testing," *51st AIAA/SAE/ASEE Joint Propulsion Conference*, AIAA Paper 2015-3825, July 2015.

[27] Walker, M. L. R., Gallimore, A. D., Boyd, I. D., and Cai, C., "Vacuum Chamber Pressure Maps of a Hall Thruster Cold-Flow Expansion," *Journal of Propulsion and Power*, Vol. 20, No. 6, 2004, pp. 1127–1131.

[28] "Vapour Vacuum Pumps – Measurements of Performance Characteristics —Part 1: Measurement of Volume Rate of Flow (Pumping Speed)," ISO 1608-1:1993, 1993.

[29] "Procedure for Measuring Speed of High-Vacuum Pumps," AVS 4.1, 1971.

[30] "Standard Practice for Ionization Gage Application to Space Simulators," ASTM E296-70, 2010.

[31] Randolph, T., Kim, V., Kaufman, H., Kozubsky, K., Zhurin, V., and Day, M., "Facility Effects in Stationary Plasma Thruster Testing," *Proceedings of the 23rd International Electric Propulsion Conference*, IEPC 1993-093, Seattle, WA, Sept. 1993.

[32] Kahn, J., Zhurin, V., Kozubsky, K., Randolph, T., and Kim, V., "Effect of Background Nitrogen and Oxygen on Insulator Erosion in the SPT-100," *Proceedings of the 23rd International Electric Propulsion Conference*, IEPC 1993-092, Seattle, WA, Sept. 1993.

[33] Rawlin, V. K., and Mantenieks, M. A., "Effect of Facility Background Gases on Internal Erosion of the 30-cm Hg Ion Thruster," *13th AIAA/*

DGLR International Electric Propulsion Conference, AIAA Paper 1978-0665, April 1978.

[34] Sengupta, A., Anderson, J. A., Garner, C., Brophy, J. R., deGroh, K. L., Banks, B. A., and Karniotis Thomas, T. A., "Deep Space 1 Flight Spare Ion Thruster 30,000 Hour Life Test," *Journal of Propulsion and Power*, Vol. 25, No. 1, Jan.–Feb. 2009, pp. 105–117.

[35] Herman, D. A., Soulas, G. C., and Patterson, M. J., "Performance Characteristics of the NEXT Long-Duration Test After 16,550 h and 337 kg of Xenon Processed," *44th AIAA/ASME/SAE/ASEE Joint Propulsion Conference & Exhibit*, AIAA Paper 2008-4527, July 2008.

[36] Nakles, M. R., and Hargus, W. A., "Background Pressure Effects on Ion Velocity Distribution within a Medium-Power Hall Thruster," *Journal of Propulsion and Power*, Vol. 27, No. 4, July–Aug. 2011.

[37] Diamant, K. D., Liang, R., and Corey, R. L., "The Effect of Background Pressure on SPT-100 Hall Thruster Performance," *50th AIAA/ASME/SAE/ASEE Joint Propulsion Conference*, AIAA Paper 2014-3710, July 2014.

[38] Burt, J. M., Josyula, E., and Boyd, I. D., "Novel Cartesian Implementation of the Direct Simulation Monte Carlo Method," *Journal of Thermophysics and Heat Transfer*, Vol. 26, No. 2, 2012, pp. 258–270.

[39] Jousten, K., and Rohl, P., "Instability of the Spatial Electron Current Distribution in Hot Cathode Ionization Gauges as a Source of Sensitivity Changes," *Journal of Vacuum Science & Technology A*, Vol. 13, No. 4, 1995, pp. 2266–2270.

[40] Arnold, P. C., and Bills, D. G., "Causes of Unstable and Nonreproducible Sensitivities in Bayard–Alpert Ionization Gauges," *Journal of Vacuum Science & Technology A*, Vol. 2, No. 2, 1984, pp. 159–162.

[41] Jenkins, R. O., "A Review of Thermionic Cathodes," *Vacuum*, Vol. 19, No. 8, 1969, pp. 353–359.

[42] Tilford, C. R., Filipelli, A. R., and Abbott, P. J., "Comments on the Stability of B–A Ionization Gauges," *Journal of Vacuum Science & Technology A*, Vol. 13, No. 2, 1995, pp. 485–487.

J. Blandino
Associate Editor